

magnetic field. A monocrystalline YIG sphere [21] of diameter 0.25 mm is glued onto the center of the CPWR where the amplitude of its magnetic field is maximal. The sample is mounted inside an oxygen-free copper sample box which is thermally anchored to the mixing chamber plate of a dilution refrigerator with a base temperature of approximately 10 mK. The position of the sample is such that it sits at the center of a superconducting magnet providing a field parallel to the length of the CPWR and in the plane of the niobium film. A schematic of the experimental setup and the room temperature microwave apparatus is shown in Fig. 1a. We are also able to measure the phase of the transmitted signal by comparing the output signal from the sample with a downconverted reference signal from the microwave source (not shown in Fig. 1).

Experiments are performed by measuring the complex transmission of the CPWR as a function of frequency, magnetic field and input signal power. Approximately 70 dB of attenuation between the output of the room-temperature microwave source and the input port of the CPWR ensures that the electrical noise temperature at the sample is comparable to the thermodynamic temperature. From the output of the CPWR, signals are amplified by approximately 40 dB at 4 K before reaching the room temperature part of the measurement instrumentation where, after mixing to an intermediate frequency and undergoing further amplification and filtering, they are digitized at 2.5 GHz using a fast data acquisition card. Measurements were typically averaged between ten thousand and one hundred thousand times.

The frequencies of the magnon modes in the YIG sphere are functions of the magnetic bias field, and can therefore be shifted by adjusting the current in the superconducting magnet. Since the plane of the CPWR is aligned parallel to the applied magnetic field, it remains superconducting up to relatively high fields, making it possible to bring a variety of magnon modes into resonance with it. By calculating the shape of the resonance microwave magnetic field of the CPWR and the magnetization within the YIG sphere for a given magnon mode, we can find their relative orientations and thus estimate the relative strength of the coupling for different magnon modes.

The microwave field of the CPWR in the region of the sphere was computed using HFSS [22] (see Fig. 2a). In contrast with the experimental geometries used in some of the previously cited works, the magnetic field of the CPWR is strongly inhomogeneous in the region around the center conductor, making it highly non-uniform in the region of the YIG sphere. This allows us to address a significant number of different magnon modes in the sphere.

The magnon modes in ferromagnetic spheres are traditionally described using three indices (n, m, r) [1], where n and m refer to the order of Legendre polynomials used

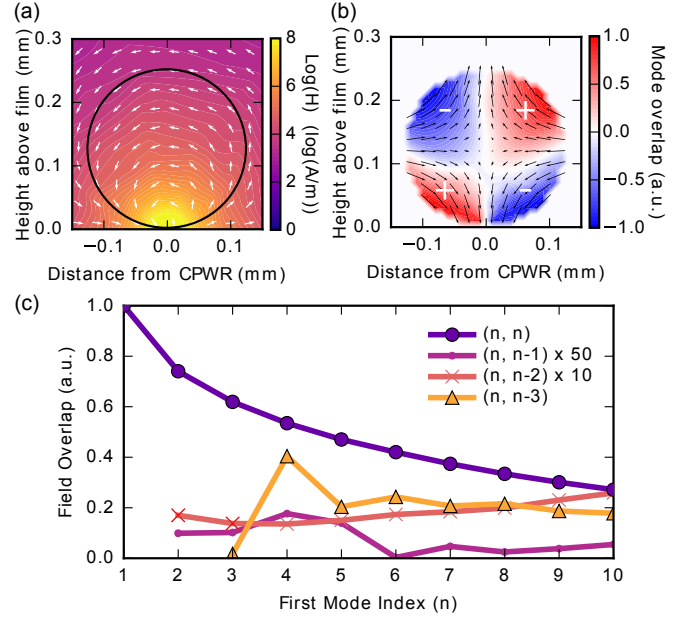


FIG. 2: (a) The microwave magnetic field distribution above the center of the CPWR. A circle of equivalent size to the YIG sphere used in the experiment is superimposed. As can be seen, the field inside the sphere is highly non-uniform. (b) The overlap of the CPWR magnetic field with the (2,2) magnon mode in the sphere. The arrows indicate the pattern of magnetization in the sphere for this mode, and the color scale reflects the dot product of the CPWR field and sphere magnetization at each point. (c) The relative coupling of four families of sphere modes with the CPWR field is estimated for values of n up to 10. Lines are guides to the eye. The $(n, n-1)$ and $(n, n-2)$ families are scaled as indicated to make them more visible. The (n, n) modes consistently couple most strongly, which remains the case for small displacements of the sphere from the center of the CPWR.

in determining the resonance condition, and r distinguishes between modes when there are multiple solutions for the same values of n and m . The mode frequencies and the associated distribution of magnetization transverse to the magnetic field can be calculated from the theory presented in [23]. None of the modes relevant to this experiment have multiple solutions so in what follows modes will simply be identified by their n and m indices. The relative coupling strength of different magnon modes can be estimated from the dot product of the magnetization with the CPWR magnetic field over the sphere, as illustrated for the (2,2) magnon mode in Fig. 2b.

The results of relative coupling calculations for magnon modes in three families up to $n = 10$ are summarised in Fig. 2c. The (n, n) modes consistently couple most strongly to the CPWR. The (1,1) mode, also known as the Kittel or ferromagnetic resonance mode has the strongest coupling of all. This mode corresponds to in phase precession of all spins in the sphere.

To observe the coupling between the YIG sphere and the CPWR experimentally, we measure the complex

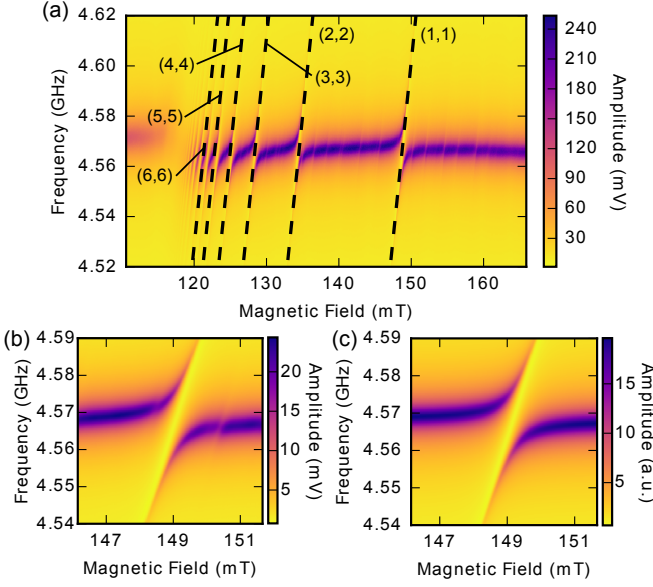


FIG. 3: (a) Experimental transmission through the CPWR as a function of frequency and applied magnetic field. Approximately ten anticrossings are visible, along with a number of weaker features. The (n, n) modes are plotted using the equations in [23] with a saturation magnetization of 170 kA/m and a constant offset to account for the effects of magnetocrystalline anisotropy. (b) A high-resolution measurement of the $(1, 1)$ anticrossing. The splitting is 16.34 MHz and two of the weaker features are also visible at higher and lower magnetic field. (c) A fit to the crossing in panel (b) using Eq. 1. The two weaker crossings are not modelled.

transmission (S_{21}) of microwave radiation through the CPWR as a function of frequency and magnetic field. The results of this experiment are summarized in Fig. 3. As the field increases above 120 mT, photons in the CPWR couple to different magnon modes in the YIG sphere and this is observed as a series of avoided crossings, with the Kittel mode, labelled $(1, 1)$ in Fig. 3a, being the most pronounced.

Apart from the Kittel mode, at least ten additional splittings are visible. As discussed above, we identify the strongly coupled modes by considering the magnetization distribution and fit their frequencies using the (n, n) mode family, which converges at high n , as seen in the data. We also observe some weakly coupled modes of similar slope attributable to other mode families in the sphere, such as those plotted in Fig. 2c.

There is good agreement between the calculated frequencies of the (n, n) modes and our experimental data up to the $(4, 4)$ mode, for a saturation magnetization of 170 kA/m. For higher modes, the observed frequencies begin to diverge from the predicted frequencies, which we attribute to the effect of magnetocrystalline anisotropy. This effect is likely to be especially significant at low temperatures as the first-order anisotropy constant of YIG is approximately three times larger near zero Kelvin than

at room temperature [24].

If the bias magnetic field is along either the hard or easy axis of the crystal, the effect of anisotropy is to shift the frequencies of all modes in the spectrum by a constant factor [25]. However, in the case of a general orientation, the effects become much more difficult to calculate and analytic expressions for the magnon mode frequencies exist for only the first few low-order modes [26]. In our experiment, it was not practical to determine and align the orientation of the crystal axes of the sphere, making it impossible to calculate the exact frequencies taking anisotropy into account. The fitted lines in Fig. 3a use only a constant offset to account for anisotropy, which works well for the first few modes. The challenge of determining the effect of the anisotropy on higher-order mode frequencies also makes it difficult to identify the weakly coupled modes observed in the data with particular mode families.

The value of 170 kA/m used for the saturation magnetization is significantly below the literature value of 197 kA/m at 4.2 K [27]. Our value is derived from the spacing of the $(1, 1)$ and $(2, 2)$ modes, where analytic expressions for the effects of anisotropy do exist. We were therefore able to calculate that anisotropy effects are not sufficient to explain this spacing, necessitating the use of a lower value of saturation magnetization in our calculations.

Figure 3b shows a high-resolution measurement of the avoided crossing between the CPWR resonance and the Kittel mode. This crossing is fitted in Fig. 3c using an equation derived from the input-output formalism [15]:

$$S_{21}(\omega) = \frac{\kappa_{ext}}{i(\omega - \omega_r) - \kappa_{ext} - \frac{\kappa_{int}}{2} + \frac{g_m^2}{i(\omega - \omega_m) - \frac{\gamma_m}{2}}} \quad (1)$$

In this fit we account for the effect of anisotropy on the frequency of the Kittel mode ω_m since an analytic expression exists. Both amplitude and phase measurements were fitted simultaneously (phase information is not plotted in Fig. 3), resulting in a linewidth of $\gamma_m = 2.97$ MHz for the Kittel mode, and internal and external linewidths of $\kappa_{int} = 1.39$ MHz and $\kappa_{ext} = 1.34$ MHz respectively for the CPWR. The coupling strength $g_m = 8.17$ MHz is larger than either of the individual linewidths, indicating that the system is in the strong coupling regime. At these magnetic fields, the CPWR frequency is shifted down slightly from its zero-field value to $\omega_r = 4.568$ GHz.

By reducing the input power, the average number of photons in the CPWR can be reduced to less than one. Even at these low powers, we are still able to detect strong coupling between CPWR photons and magnon modes (see Fig. 4a), demonstrating the potential of the system in the context of quantum information processing.

We can also excite the YIG-CPWR system with a short square pulse having a carrier frequency between the two split levels (e.g. 4.570 GHz at 149 mT). After such a

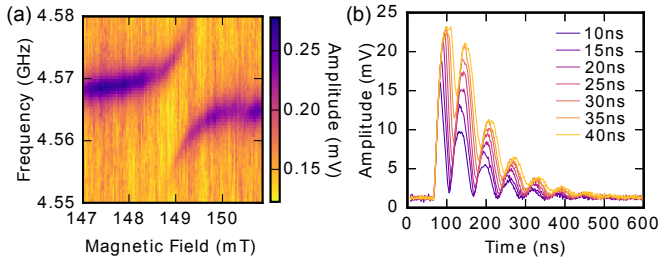


FIG. 4: (a) Measurement of the avoided crossing between the Kittel mode and the CPWR at very low input powers. (b) Time response of the system to a square pulse of varying length when the YIG sphere and the CPWR are tuned to be resonant. Beating in the output signal is at the frequency of the level splitting.

pulse, we see oscillations in the output signal with frequency equal to the splitting. The temporally narrow square pulse has a sufficiently wide frequency spectrum to simultaneously excite both levels, so that these oscillations are interpreted as being due to beating between the two levels. This interpretation is reinforced by the reduction in amplitude of the oscillations as the pulse length increases, reducing its spectral width.

In summary, we have demonstrated strong coupling of a magnonic resonator, consisting of a sphere of yttrium-iron garnet, to a coplanar waveguide resonator typical of those used in circuit QED experiments. The coupling strength of 8.17 MHz for the Kittel mode is in the strong coupling regime, and we have also shown strong coupling to a series of other non-uniform modes of oscillation in the YIG sphere, which were identified as the (n, n) modes.

The range and tunability of excitations available in magnonic systems presents interesting possibilities for building hybrid quantum systems. As this work shows that a planar superconducting resonator can be coupled strongly to a YIG sphere, it implies that it should likewise be possible to integrate it with planar superconducting quantum bits, giving access to a wide variety of high-fidelity control and measurement techniques. As such, this work represents an important step towards the development of exciting new architectures for quantum magnonic systems.

This work was supported by Engineering and Physical Sciences Research Council grant EP/K032690/1. S. Kosen would also like to thank the Indonesia Endowment Fund for Education for its support.

* Electronic address: richard.morris@physics.ox.ac.uk

- [1] L. R. Walker, Phys. Rev. **105**, 390 (1957), URL <http://dx.doi.org/10.1103/PhysRev.105.390>.
- [2] R. W. Damon and J. R. Eshbach, Journal of Applied Physics **31**, S104 (1960), URL <http://scitation.aip.org/content/aip/journal/>

- jap/31/5/10.1063/1.1984622.
- [3] V. Cherepanov, I. Kolokolov, and V. L'vov, Physics Reports **229**, 81 (1993), URL [http://dx.doi.org/10.1016/0370-1573\(93\)90107-0](http://dx.doi.org/10.1016/0370-1573(93)90107-0).
- [4] A. V. Chumak, V. I. Vasyuchka, A. A. Serga, and B. Hillebrands, Nat Phys **11**, 453 (2015), URL <http://dx.doi.org/10.1038/nphys3347>.
- [5] J. Adam and J. Collins, Proceedings of the IEEE **64**, 794 (1976), URL <http://dx.doi.org/10.1109/PROC.1976.10214>.
- [6] *Spin Waves: Theory and Applications* (Springer Nature, 2009), URL <http://dx.doi.org/10.1007/978-0-387-77865-5>.
- [7] Y. Tabuchi, S. Ishino, A. Noguchi, T. Ishikawa, R. Yamazaki, K. Usami, and Y. Nakamura, Comptes Rendus Physique **17**, 729 (2016), URL <http://dx.doi.org/10.1016/j.crhy.2016.07.009>.
- [8] X. Zhang, C.-L. Zou, L. Jiang, and H. X. Tang, Phys. Rev. Lett. **113** (2014), URL <http://dx.doi.org/10.1103/PhysRevLett.113.156401>.
- [9] M. Goryachev, W. G. Farr, D. L. Creedon, Y. Fan, M. Kostylev, and M. E. Tobar, Phys. Rev. Applied **2**, 054002 (2014), URL <http://link.aps.org/doi/10.1103/PhysRevApplied.2.054002>.
- [10] J. Bourhill, N. Kostylev, M. Goryachev, D. L. Creedon, and M. E. Tobar, Phys. Rev. B **93**, 144420 (2016), URL <http://link.aps.org/doi/10.1103/PhysRevB.93.144420>.
- [11] N. Kostylev, M. Goryachev, and M. E. Tobar, arXiv:1508.04967v3 (2016), URL <http://arxiv.org/abs/1508.04967>.
- [12] N. J. Lambert, J. A. Haigh, and A. J. Ferguson, J. Appl. Phys. **117**, 053910 (2015), URL <http://dx.doi.org/10.1063/1.4907694>.
- [13] N. J. Lambert, J. A. Haigh, S. Langenfeld, A. C. Doherty, and A. J. Ferguson, Phys. Rev. A **93** (2016), URL <http://dx.doi.org/10.1103/PhysRevA.93.021803>.
- [14] X. Zhang, C. Zou, L. Jiang, and H. X. Tang, Journal of Applied Physics **119**, 023905 (2016), URL <http://scitation.aip.org/content/aip/journal/jap/119/2/10.1063/1.4939134>.
- [15] Y. Tabuchi, S. Ishino, T. Ishikawa, R. Yamazaki, K. Usami, and Y. Nakamura, Phys. Rev. Lett. **113**, 083603 (2014), URL <http://link.aps.org/doi/10.1103/PhysRevLett.113.083603>.
- [16] D. Zhang, X.-M. Wang, T.-F. Li, X.-Q. Luo, W. Wu, F. Nori, and J. Q. You, Npj Quantum Information **1**, 15014 (2015), URL <http://dx.doi.org/10.1038/npjqi.2015.14>.
- [17] Y. Tabuchi, S. Ishino, A. Noguchi, T. Ishikawa, R. Yamazaki, K. Usami, and Y. Nakamura, Science **349**, 405 (2015), ISSN 0036-8075, URL <http://science.sciencemag.org/content/early/2015/07/08/science.aaa3693>.
- [18] H. Huebl, C. W. Zollitsch, J. Lotze, F. Hocke, M. Greifenstein, A. Marx, R. Gross, and S. T. B. Goennenwein, Phys. Rev. Lett. **111**, 127003 (2013), URL <http://link.aps.org/doi/10.1103/PhysRevLett.111.127003>.
- [19] L. DiCarlo, J. M. Chow, J. M. Gambetta, L. S. Bishop, B. R. Johnson, D. I. Schuster, J. Majer, A. Blais, L. Frunzio, S. M. Girvin, et al., Nature **460**, 240 (2009), URL <http://dx.doi.org/10.1038/nature08121>.
- [20] A. Blais, R.-S. Huang, A. Wallraff, S. M. Girvin, and R. J. Schoelkopf, Phys. Rev. A **69** (2004), URL <http://dx.doi.org/10.1103/PhysRevA.69.012306>.

- [//dx.doi.org/10.1103/PhysRevA.69.062320](http://dx.doi.org/10.1103/PhysRevA.69.062320).
- [21] URL <http://www.ferrisphere.com/>.
 - [22] Ansys, *Electromagnetics suite*, release 16.0.0, build 2014-11-21 00:25:49.
 - [23] P. C. Fletcher and R. O. Bell, J. Appl. Phys. **30**, 687 (1959), URL <http://dx.doi.org/10.1063/1.1735216>.
 - [24] P. Hansen, Journal of Applied Physics **45**, 3638 (1974), URL <http://scitation.aip.org/content/aip/journal/jap/45/8/10.1063/1.1663830>.
 - [25] A. Gurevich and G. Melkov, *Magnetization Oscillations and Waves* (CRC Press, Inc, 1996).
 - [26] I. H. Solt and P. C. Fletcher, Journal of Applied Physics **31**, S100 (1960), URL <http://scitation.aip.org/content/aip/journal/jap/31/5/10.1063/1.1984620>.
 - [27] P. Hansen, P. Roeschmann, and W. Tolksdorf, J. Appl. Phys. **45**, 2728 (1974), URL <http://dx.doi.org/10.1063/1.1663657>.